JACS
JOURNAL OF THE AMERICAN CHEMICAL SOCIETY
Article
pubs.acs.org/JACS

Potential Gradient and Photocatalytic Activity of an Ultrathin p−n Junction Surface Prepared with Two-Dimensional Semiconducting Nanocrystals

Shintaro Ida,*[,†,‡,§] Akihide Takashiba,[†] Shota Koga,[†] Hidehisa Hagiwara,[†,‡] and Tatsumi Ishihara[†,‡]

[†]Department of Applied Chemistry, Faculty of Engineering, Kyushu University, 744 Motooka, Nishi-ku, Fukuoka 819-0395, Japan
[‡]International Institute for Carbon Neutral Energy Research (I2CNER), Kyushu University, Motooka 744, Nishi-ku, Fukuoka 819-0395, Japan
[§]PRESTO, Japan Science and Technology Agency (JST), 4-1-8 Honcho, Kawaguchi, Saitama 332-0012, Japan

Supporting Information

ABSTRACT: The creation of p−n junction structure in photocatalysts is a smart approach to improve the photocatalytic activity, as p−n junctions can potentially act to suppress the recombination reaction. Understanding the surface conditions of the junction parts is one of the biggest challenges in the development of photocatalyst surface chemistry. Here, we show a relationship between the photocatalytic activity and potential gradient of the junction surface prepared from two-dimensional crystals of p-type NiO and n-type calcium niobate (CNO). The ultrathin (ca. 2 nm) junction structure and the surface potential were analyzed using low energy ion scattering spectroscopy and Kelvin probe force microscopy. The photocatalytic H_2 production rate for the n−p (CNO/NiO) junction surface was higher than those for p−n (NiO/CNO) junction, p, and n surfaces. The surface potential of the CNO/NiO junction part (surface: CNO) was lower than that of the CNO crystals in the same CNO crystal surface. These potential gradients result in specially separated reaction sites, which suppress the recombination reaction in the CNO nanosheet. Photo-oxidation and photoreduction sites in the junction structure were confirmed using the photodeposition reaction of MnO_x and Ag.

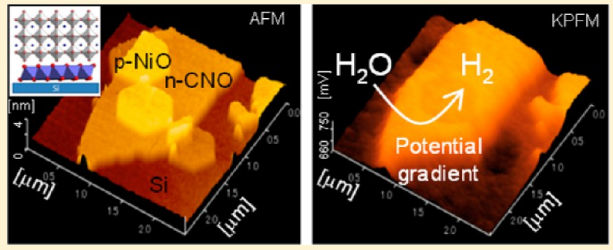

INTRODUCTION

Photocatalytic decomposition of water using semiconducting materials is certainly seen as one of the key players in the ultimate renewable energy system based solely on water and solar.[1−12] The creation of p−n junction structure in photocatalysts is a smart approach to improve the photocatalytic activity, as p−n junctions can potentially act to suppress the recombination reaction.[13−22] On the surface of a photocatalyst with the p−n junction structure, it is considered that the surface potential has a gradient at the junction parts due to the diffusion of charge carriers (hole and/or electrons). The difference in the surface potential is expected to create spatially separated oxidation and reduction sites on the surface. However, the advancement in this field has been limited due to the difficulty in the preparation and evaluation of such junction structures to understand the actual condition and function of p−n junction surface on the photocatalytic activity. Understanding such a surface condition of p−n junction will open a new era in photocatalyst surface chemistry. Here, we show a relationship between the photocatalytic activity and potential gradient of a junction surface prepared from two-dimensional (2D) crystals of p-type nickel oxide (NiO) and n-type calcium niobate (CNO). The compositional depth profile of approximately 2 nm thick junction structure was confirmed by low energy ion scattering (LEIS) spectroscopy, an innovative technique which can provide accurate compositional information on the very first atomic layer of a material surface.[23,24] The photocatalytic activity on the n−p junction surface was higher than those on the p−n junction or p and n surfaces, verifying the strong influence of the junction structure. Kelvin probe force microscopy images showed that the surface potential of the CNO/NiO junction part (crystal surface: CNO) was higher than that of the NiO crystals and lower than that of the CNO crystals in the same CNO crystal surface, creating potential gradients on the same CNO film surface. These potential gradients produce spatially separated reaction sites, which function to suppress the recombination reaction.

The preparation of ultrathin p−n junctions from two materials with a large lattice mismatch by chemical vapor deposition (CVD) is generally difficult, so that crystal lattice strain or a decrease in crystallinity would be generated in the vicinity of the interface. Therefore, the p−n junction examined in this investigation was prepared by the lamination of p-type NiO and n-type CNO 2D crystal. The model structures of NiO and CNO 2D crystals are shown in Figure 1. The NiO 2D crystal has the same crystal structure as a one-NiO_6-unit layer of the (111) plane in bulk NiO. The NiO 2D crystal has a

Received: September 12, 2013
Published: January 6, 2014

   dx.doi.org/10.1021/ja409465k | J. Am. Chem. Soc. 2014, 136, 1872−1878

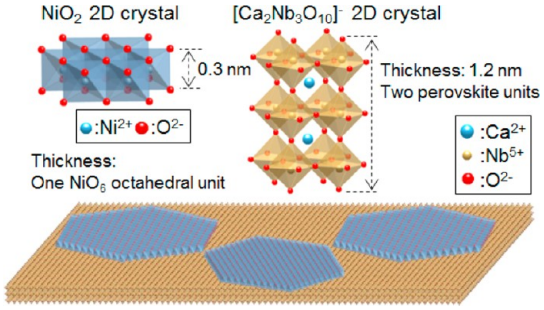

Figure 1. Model structures of p-type NiO, n-type CNO crystals, and a p-NiO/n-CNO junction.

perovskite structure with A-site Ca^{2+} and B-site Nb^{5+}, and there are two perovskite units in the thickness direction.[25]

EXPERIMENTAL SECTION

Materials. $Ni(NO_3)_2{\cdot}6H_2O$ (>98.0% Wako Pure Chemical Industries Ltd.), $CH_3(CH_2)_{11}OSO_3Na$ (>99.0% Kishida Chemical Co. Ltd.), $C_6H_{12}N_4$ (>99.0% Wako Pure Chemical Industries Ltd.), $K(OOCCH_3)$ (>97.0% Kishida Chemical Co. Ltd.), $Ca(OOCCH_3)_2{\cdot}0.5H_2O$ (>99.0% Kishida Chemical Co. Ltd.), Nb_2O_5 (>99.9% Wako Pure Chemical Industries Ltd.).

Preparation of p–n and n–p Junction Films. $Ca_2Nb_3O_{10}$ and nickel hydroxide 2D crystals were prepared by exfoliation of $KCa_2Nb_3O_{10}$ and layered nickel hydroxides intercalated with dodecyl sulfate, respectively.[25,26] 2D crystal films were prepared by the Langmuir–Blodgett method. Si(100) wafer and quartz glass were used as substrates. Nickel hydroxide or $Ca_2Nb_3O_{10}$ 2D crystal suspension (3 mL) were diluted with 296 mL of Milli-Q water and poured into a trough. After 30–50 min, a moving barrier was used to compress the surface of the solution at a rate of 0.6 mm/s until the surface pressure reached 10–15 mN/m. This resulted in a nickel hydroxide or $Ca_2Nb_3O_{10}$ 2D crystals floating at the liquid/air interface, which were then transferred onto a substrate by horizontal immersion of the substrate. This procedure was repeated two times to fabricate the multilayer film of nickel hydroxide and $Ca_2Nb_3O_{10}$ 2D crystals. The films were heated at 400 °C for 1 h in air to convert nickel hydroxide into NiO.

Photocatalytic Water Splitting. The photocatalytic decomposition of water was performed using a conventional closed circulating system. The p–n and n–p junction films deposited on a quartz glass substrate were placed in 20 mL of aqueous 10 vol % methanol solution. A quartz reaction cell was irradiated by an external light source consisting of a 300 W Xe lamp. During photodecomposition, the solution was mixed using a magnetic stirring bar. Ar gas (initial pressure: 18 kPa) was used as the circulating carrier gas. The H_2 gas generated in the photocatalytic reaction was measured by gas chromatography with a thermal conductivity detector (Shimadzu Corp., GC-8A).

Characterization and Equipment. The thickness of the exfoliated nanosheets was measured by atomic force microscopy (AFM) (Seiko, Nanocute). Transmission electron microscopy (TEM) and selective area electron diffraction patterns of nanosheets were obtained using JEOL JEM2400 microscopes. Low energy ion scattering (LEIS) spectra were obtained using an ION-TOF Q-tac^{100} instrument. For LEIS analysis, the sample surface (1.7 × 1.7 mm^2) is bombarded with $^4He^+$ ions at an energy of 3 keV. The ions are scattered by the surface atoms according to the laws of the conservation of energy and momentum. The masses of the scattering surface atoms are determined by measuring the energy of the backscattered ions. AFM and Kelvin probe force microscopy (KPFM) observations were performed using an environment control type probe microscope system (Seiko Instruments: E-sweep) under vacuum conditions. The KPFM images were obtained after UV-light irradiation for 15 min. A Rh-coated AFM tip was used for the observation. Auger spectra mapping images of 2D crystal film were obtained using Auger electron spectroscopy (JEOL). The photodeposition reaction of MnO_x and Ag was performed in 0.1 M $AgNO_3$ and 0.1 M $MnSO_4$ aqueous solution under UV-light irradiation for 30 min using an UV lamp (254 nm, 16 W) in order to confirm which parts of the junction films are photo-oxidation and photoreduction sites. Photoelectrochemical experiments were carried out in 0.1 M Na_2SO_4 aqueous solution using a conventional three-electrode system with a Pt counter electrode and a saturated Ag/AgCl reference electrode under chopped light illumination (300 W Xe lamp).

RESULTS AND DISCUSSION

Figure 2a shows a TEM image of the p–n (NiO/CNO) junction part that was prepared by heating the junction part of

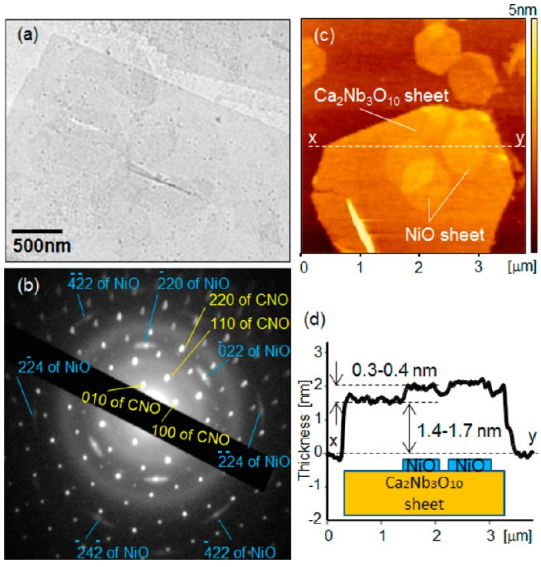

Figure 2. (a) TEM image, (b) SAED pattern, (c) AFM image, and (d) cross-sectional profile of the AFM image of the p–n junction part of p-NiO crystals on n-CNO crystals.

nickel hydroxide and CNO crystals deposited on a TEM grid at 400 °C. In this heat treatment, the nickel hydroxide crystals were converted to NiO single crystals. Although there was little difference in the contrast between the NiO and CNO sheets due to their thickness, hexagonal (NiO) and polygonal (CNO) shapes were confirmed in the TEM image. The crystallinity of the junction part was analyzed using selected area electron diffraction (SAED). Figure 2b shows a SAED pattern of the p–n junction part. Square-shaped patterns were assigned to the 100, 010, 110, and 220 diffractions of [001]-oriented CNO crystal, while hexagonal-shaped patterns were assigned to the $2\bar{2}0$, $0\bar{2}2$, and $4\bar{2}\bar{2}$ diffractions of [111]-oriented NiO crystal. This indicates that the CNO and NiO crystals are single crystals. Thus, the two types of diffraction patterns observed indicate that the p–n junction structure consists of two different 2D single crystals. The thickness of the p-NiO crystal estimated from the AFM image was ca. 0.3–0.4 nm and that of the n-CNO crystal was 1.4–1.7 nm, so that the total thickness of the p–n junction part was around 2.0 nm, as shown in Figure 2c and d. Junction films of NiO and CNO crystals were prepared by the Langmuir–Blodgett method. Figure 3 shows the FE-SEM images of monolayer CNO, NiO crystal film, CNO/NiO junction, and NiO/CNO junction film. Although the Si substrate was not fully covered with 2D crystals, monolayer crystals were deposited on the Si substrate because

dx.doi.org/10.1021/ja409465k | J. Am. Chem. Soc. 2014, 136, 1872–1878

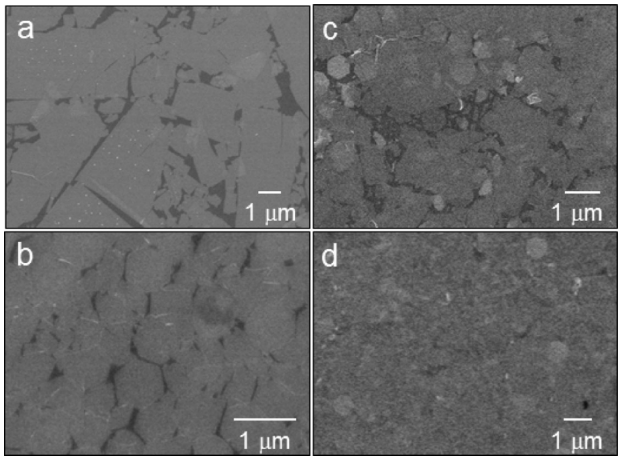

Figure 3. FE-SEM images: (a) monolayer CNO crystal film, (b) monolayer NiO crystal film, (c) CNO/NiO junction film (n–p junction, CNO crystal surface), and (d) NiO/CNO junction film (p–n junction, NiO crystal surface) on Si substrate.

the contrast of the 2D crystal in the FE-SEM image was homogeneous.

Figure 4 shows LEIS spectra of monolayer NiO and CNO crystal films and junction films of CNO/NiO and NiO/CNO.

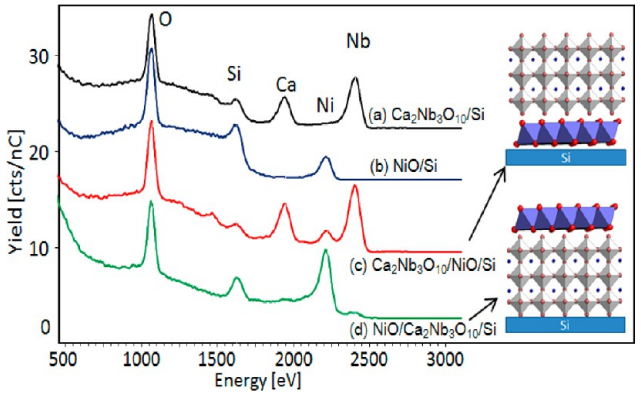

Figure 4. 3 keV $^4He^+$ LEIS spectra: (a) monolayer CNO crystal film, (b) monolayer NiO crystal film, (c) CNO/NiO junction film (n–p junction, CNO crystal surface), and (d) NiO/CNO junction film (p–n junction, NiO crystal surface) on Si substrate.

The peak of Si is due to the substrate at the surface. The NiO film contained Ni and O, whereas the CNO film contained Ca, Nb, and O. The CNO/NiO (CNO crystal surface) spectrum has peaks assigned to Ca, Nb, and O but also a peak assigned to Ni, although the intensity of the Ni peak was less than that in the spectrum of only the NiO film (Figure 4c). This indicates that most of the NiO crystals are covered with CNO crystals. On the other hand, the LEIS spectrum for the NiO/CNO (NiO crystal surface) film showed a strong Ni peak, which was the same spectrum as that for only the NiO film (Figure 4d). In contrast, the peak intensities for Ca and Nb from the CNO crystals that were located under the 0.3 nm thick NiO were very weak. This result confirms that real information on the surface composition can be obtained using the LEIS technique.

Figure 5a shows a LEIS spectral depth profile for a NiO/$Ca_2Nb_3O_{10}$/Si film. By sputtering of the surface using $^{40}Ar^+$/500 eV (110 nA target current, 2 × 2 mm^2 analysis area, 5 s cycle time), the intensity of the Ca and Nb peaks increased.

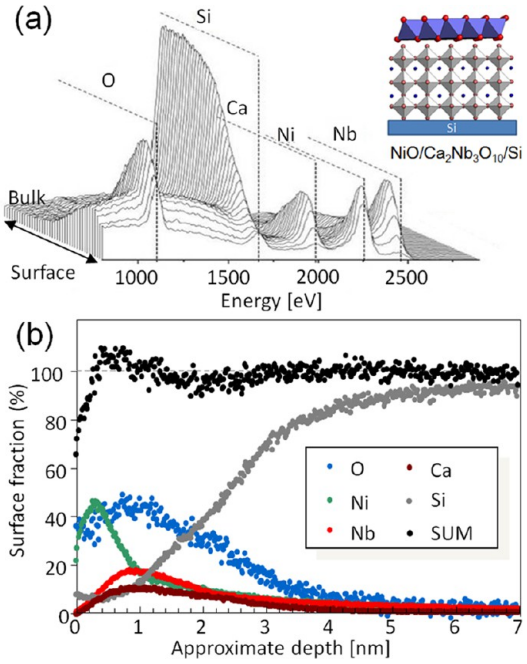

Figure 5. (a) 3 keV $^4He^+$ LEIS spectral depth profile for a NiO/$Ca_2Nb_3O_{10}$/Si film. (b) Surface fractions for the various elements in the 3 keV $^4He^+$ LEIS spectra as a function of ion dose for the NiO/$Ca_2Nb_3O_{10}$/Si film.

LEIS is an inherently quantitative technique, and the signals are proportional to the surface fractions; therefore, the ratio of the surface chemical composition can be estimated from the LEIS spectral intensities. Figure 5b shows the elemental fractions for the surface from the LEIS spectra as a function of ion dose. The ratio of the Ni and O surface fractions before sputtering was around 1:1, while the ratio of the Ca and Nb surface fractions after 1 nm sputtering was around 2:3, which corresponds to the chemical composition ratios of NiO and CNO($Ca_2Nb_3O_{10}$), respectively. These LEIS spectra indicate that an ultrathin p–n junction was successfully prepared by the deposition of p-type and n-type 2D crystals.

Figure 6 shows time courses for photocatalytic H_2 production from p-NiO, n-CNO, NiO/CNO (p–n), and

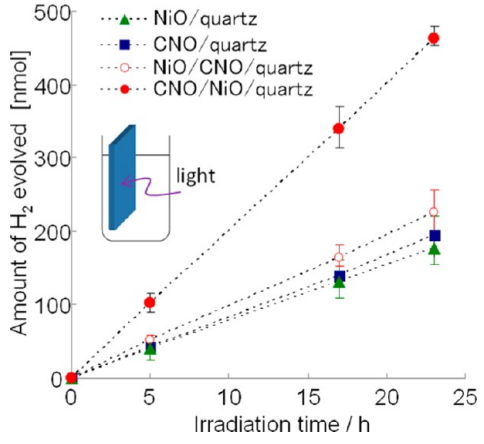

Figure 6. Time courses of H_2 production from p-NiO, n-CNO, NiO/CNO (p–n), and CNO/NiO (n–p) junction films on quartz substrates in an aqueous solution of 10 vol % methanol under 300 W Xe lamp irradiation.

dx.doi.org/10.1021/ja409465k | J. Am. Chem. Soc. 2014, 136, 1872–1878

CNO/NiO (n−p) junction films on quartz substrates. In this system, methanol acts as a sacrificial reagent for the photooxidation reaction, and hydrogen is generated by the photoreduction of water. Each test was repeated three or four times. Hydrogen was generated from all the films examined. The hydrogen production rate for the films was in the order of n−p junction film > p−n junction film > n-CNO film > p-NiO film. It is interesting that the production rate of the n−p junction film (CNO surface) was 2 times larger than that of the p−n junction (NiO surface) film, while that of the p−n junction film was almost the same as that of the n-CNO film. The main part of the n−p junction film surface was CNO crystals, as with the n-CNO film. However, the production rate of the n−p junction film was 2 times as large as that of the n-CNO film. These results indicate that the photocatalytic activity is influenced by not only the surface crystal structure and composition but also the crystal structure and composition under the surface. The CNO/NiO junction film was not a perfect film because some parts in the film were only CNO crystals, while other parts were CNO crystals with NiO crystals under the layer (n−p junction parts). However, the photocatalytic activity of the CNO/NiO (n−p) junction film was higher than those of the NiO crystal and CNO crystal films. Thus, the improvement of photocatalytic activity may be due to a junction effect. In the case of ultrathin semiconducting film (<2 nm), molecular orbital theory and/or solid state theory are used to discuss the physical phenomenon of nanosheet p−n junction film. In the preset report, we used solid state theory to discuss the results. When a p-type semiconductor is in contact with an n-type semiconductor, free carriers generally diffuse at the interface to balance the Fermi levels of both materials at the junction part, which results in a change of the surface potential (Fermi level). Therefore, it would be expected that the surface potentials of the CNO/NiO junction parts are different from those of the only CNO crystal parts in the CNO/NiO junction film.

Figure 7 shows AFM and Kelvin probe force microscopy (KPFM) images of the CNO/NiO (n−p) and NiO/CNO (p−n) junction parts under vacuum conditions. The CNO and NiO crystals were intentionally deposited with low coverage on the substrate to assist clarification of the surface characteristics, as shown in Figure 7a and d. The KPFM images (Figure 7b and e) show light (high surface potential) and dark (low surface potential) parts, which indicate shallow and deep Fermi levels, respectively.[27,28] Considering the difference in the surface potential between the CNO and NiO crystals, the parts of only NiO crystals are darker than those of only CNO crystals. This image provides information regarding the relationship between the Fermi levels of n-CNO and p-NiO crystals. Parts c and f of Figure 7 show cross-sectional profiles of the junction part in AFM and KPFM images. The surface potential of the CNO/NiO or NiO/CNO junction part is higher than that of the NiO crystals and lower than that of the CNO crystals. It should be noted that the surface potential is not affected by the height of the material (low: NiO crystal < CNO crystal < CNO/NiO = NiO/CNO junction part: high) but is affected by the underlying material (junction structure).

In general, the diffusion of carriers continues until the drift current balances the diffusion current. In the case of ultrathin film, there is not enough space to form the depletion region that is formed in a general p−n junction device. However, the electrons and holes diffuse across the junction into the p-type NiO/n-type CNO nanosheets to balance the Fermi level as

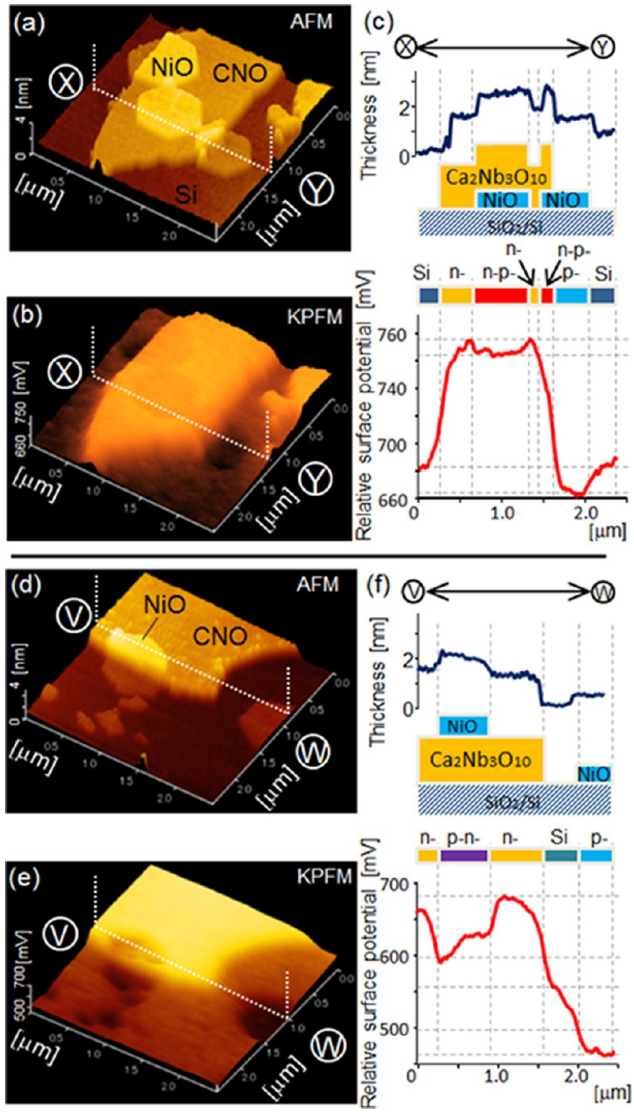

Figure 7. (a) AFM image, (b) KPFM images, and (c) cross-sectional profile between X and Y of the CNO/NiO (n−p) junction film under vacuum conditions. (d) AFM image, (e) KPFM images, and (f) cross-sectional profile between V and W of the NiO/CNO (p−n) junction film under vacuum conditions.

long as carriers such as electrons and holes exist in n-type CNO and p-NiO nanosheets. Therefore, in the region of an ultrathin p−n junction (2 nm), it is possible to assume that all donors and acceptors are fully ionized. This means that the carrier concentration in the CNO and NiO sheets decreases in the ultrathin p−n junction region. It is known that the position of the Fermi level varies as a function of carrier concentration and obeys

$$\text{n-type semiconductor: } E_F = E_C - kT \ln(n_0/N_C) \quad (1)$$

$$\text{p-type semiconductor: } E_F = E_V + kT \ln(p_0/N_V) \quad (2)$$

where E_F is the Fermi level, E_C is the conduction band level, E_V is the valence band level, k is the Boltzmann constant, N_C is the effective density of conduction band states, N_V is the effective density of valence band states, n_0 is the thermal-equilibrium concentration of electrons, p_0 is the thermal-equilibrium concentration of holes, and T is the temperature. When the carrier concentration in the CNO/NiO junction part decreases,

dx.doi.org/10.1021/ja409465k | J. Am. Chem. Soc. 2014, 136, 1872−1878

the position of the Fermi level in the ultrathin p−n junction part becomes lower than that of CNO and becomes higher than that of NiO. Thus, the position of the Fermi level in the ultrathin p−n junction part locates the positions between the Fermi level of the CNO and NiO nanosheet. The difference in the surface potentials (position of Fermi level) obtained from KFM images of CNO/NiO and NiO/CNO substrates, as shown in Figure 7, corresponded to the theoretically-estimated Fermi level.

In the case of the CNO/NiO junction film, most parts of the surface are CNO crystals. However, there are high and low surface potential parts in the same surface of CNO crystals, because there are junction parts and nonjunction parts. Thus, potential gradients are generated in the same surface of CNO crystals. It is probable that these potential gradients result in spatially separated reaction sites (oxidation and reduction sites), which may suppress the recombination reaction. The reason for the lower activity of the NiO/CNO junction film than that of the CNO/NiO film may be because the photocatalytic activity of the surface of NiO crystal is lower than that of the surface of CNO crystal. This indicates that material design to control the potential gradient on the catalyst surface is necessary to obtain highly efficient photocatalysts.

The photodeposition reaction of MnO_x and Ag in 0.1 M $AgNO_3$ and 0.1 M $MnSO_4$ aqueous solution was performed to confirm which parts of the junction films are photo-oxidation and photoreduction sites. In this reaction, Mn^{2+} is oxidized to Mn_2O_3 or MnO_2 by photogenerated holes, while Ag^+ is reduced to Ag by photogenerated electrons. MnO_x and Ag are deposited at the oxidation and reduction sites during the photocatalytic reaction. Although the deposition parts of Mn_2O_3 and Ag are not always oxidation and reduction sites of water, we can discuss the tendency of the charge transfer of generated carriers in the photocatalytic reaction.

Figure 8 shows FE-SEM images of the CNO/NiO junction films after the photocatalytic deposition reaction. MnO_x particles were deposited on junction parts and/or their edges, while Ag particles were deposited on CNO in the nonjunction part. There was no deposited material on NiO in the nonjunction part. Figure 9a shows an Auger spectra mapping image of Ag for the CNO/NiO junction surface after the photodeposition reaction of Ag. The intensity of the Ag signal of the nonjunction part was stronger than that of the junction part, indicating that the Ag particle is likely to be deposited on CNO in the nonjunction part. In the case of the photodeposition of MnO_x, the intensity of the Mn signal of the junction part was stronger than that of the nonjunction part, as shown in Figure 9b. These results indicate that the CNO/NiO junction parts are the photo-oxidation site, while the nonjunction parts and/or their edges are the photoreduction site. The potential gradient in the CNO crystal might result in specially separated reaction sites. On the other hand, in the case of NiO/CNO junction film, both Ag and MnO_x particles were deposited on the CNO sheet (nonjunction part). In addition, there is no deposited material on the NiO sheet (nonjunction part), as shown in Figure S2 of the Supporting Information. The surface of the NiO sheet might not be active for the photodeposition reaction of Ag and MnO_x. Thus, in the case of the NiO/CNO (p−n) junction surface, it is considered that the photodeposition reaction was not suitable to confirm the photo-oxidation and photoreduction sites.

Figure 10 shows a proposal mechanism for the photodeposition reactions of Ag and MnO_x on the CNO/NiO (n−p)

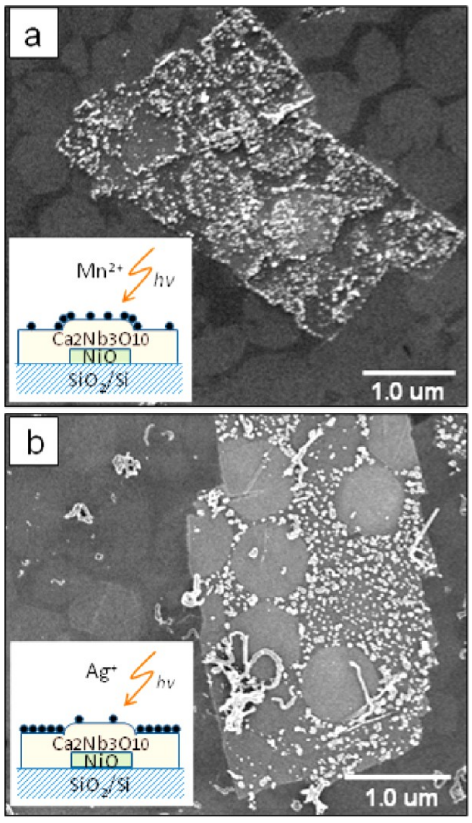

Figure 8. FE-SEM images of CNO/NiO junction parts after photodeposition reaction in (a) 0.1 M $MnSO_4$ and (b) 0.1 M $AgNO_3$ aqueous solutions.

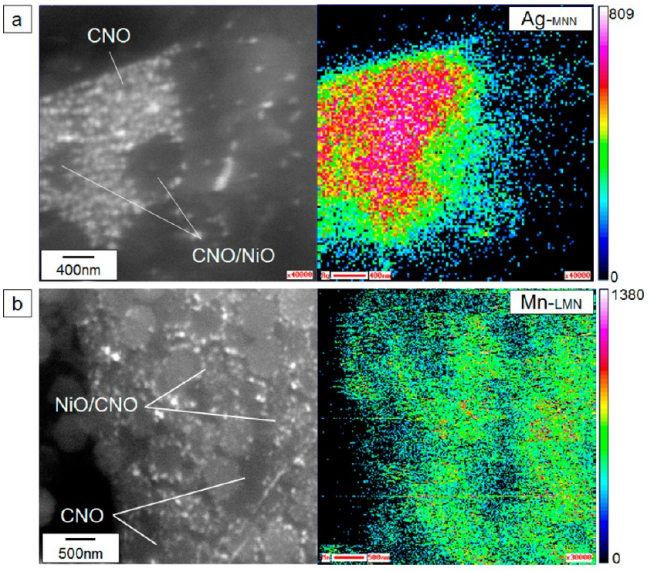

Figure 9. Auger spectra mapping images of the CNO/NiO junction part after photodeposition reaction: (a) SEM and Ag signal images after the photodeposition reaction in 0.1 M $AgNO_3$ aqueous solutions and (b) SEM and Mn signal images after the photodeposition reaction in 0.1 M $MnSO_4$ aqueous solutions.

junction surface. In the region of an ultrathin p−n junction (2 nm), it is possible to assume that all donors and acceptors are fully ionized. In addition, ionized donors are left in the narrow region of the nonjunction part close to the junction edge due to the diffusion of carriers, as shown in Figure 10a. These ionized

dx.doi.org/10.1021/ja409465k | J. Am. Chem. Soc. 2014, 136, 1872−1878

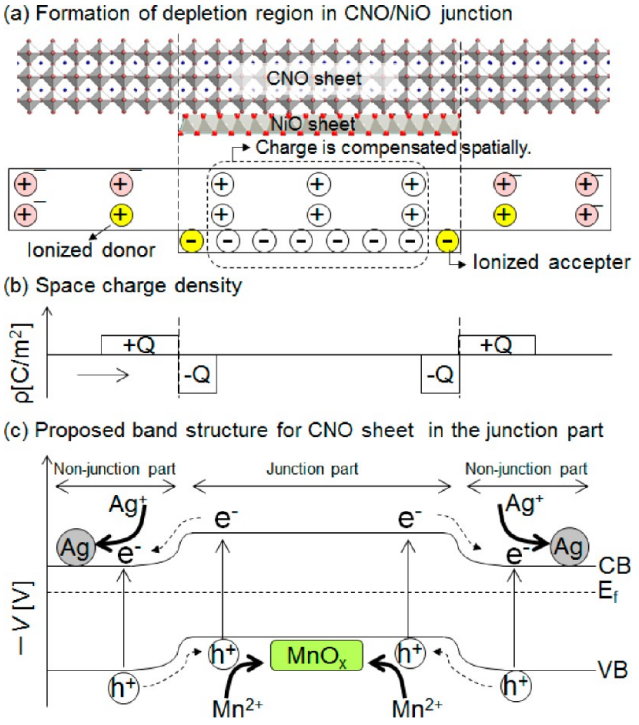

Figure 10. Proposed band structure model in horizontal direction to the CNO/NiO junction surface: (a) formation of a depletion region in the CNO/NiO junction, (b) space charge density remaining in the CNO/NiO junction surface, and (c) the model of band structure for CNO sheet in the junction and nonjunction region.

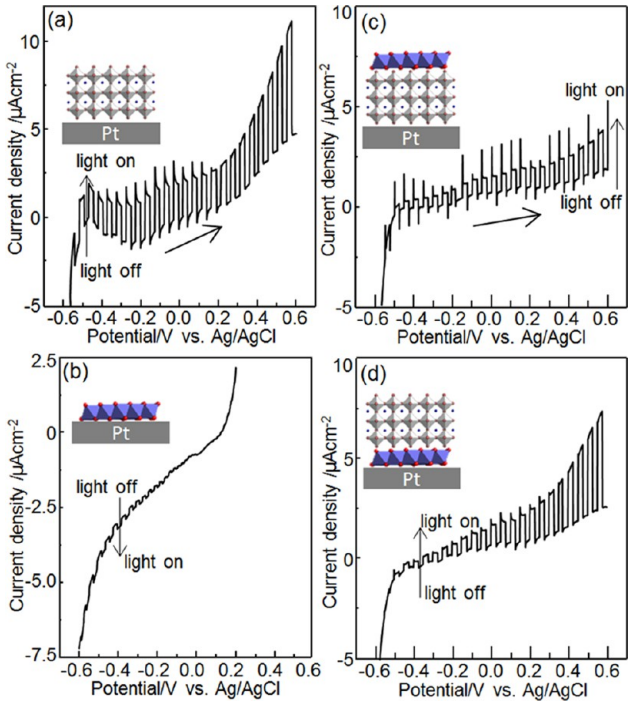

Figure 11. Current−potential curves in a 0.1 M Na_2SO_4 aqueous solution under chopped irradiation (300 W Xe lamp) for the nanosheet junction and nonjunction films deposited on a Pt surface (Pt/Ti/SiO_2/Si substrate): (a) CNO nanosheet film, (b) NiO nanosheet film, (c) NiO/CNO junction film, and (d) CNO/NiO junction film.

donors and acceptors make a difference in the space charge density around the edge of the junction part, while the space charge density of the junction part in the horizontal direction to the substrate is zero because the charges of the ionized donors and acceptors in the junction part are spatially compensated with each other, as shown in Figure 10b. The two regions of immobile positive and negative charges around the edge of the junction part might result in an electric field and band bending in the same CNO nanosheet, as shown in Figure 10c. The photoexcited electrons and holes in the CNO nanosheet are separated by the intraband bending. The photoexcited electrons move to the nonjunction part (photoreduction site), and the photoexcited holes move to the junction part (photo-oxidation site). The band structure proposed in Figure 10c is in good agreement with the KPFM image of the CNO/NiO junction part, as shown in Figure 7b.

Figure 11 shows current−potential curves in a 0.1 M Na_2SO_4 aqueous solution under UV-light illumination for the junction and nonjunction films deposited on a Pt surface. The photo-oxidation and photoreduction currents were observed from the CNO and NiO monolayer films, respectively. On the other hand, both junction films (NiO/CNO and CNO/NiO) showed photo-oxidation currents. The onset potentials (< -0.6 V) of the photo-oxidation current for the CNO/NiO and NiO/CNO junction films were almost the same as that of CNO monolayer film. One of the possible reasons for this result is that the number of free carriers in the CNO nanosheet (1.4 nm) might be larger than that of the NiO nanosheet (0.3 nm). Thus, the contribution to the band structure in the nanosheet p−n junction of the mono CNO nanosheet might be greater than that of the mono NiO nanosheet. In order to discuss the band structure for the nanosheet junction such as CNO/NiO and NiO/CNO, fundamental physical properties such as carrier concentration and dielectric constant of mono CNO and NiO nanosheets are necessary. However, fundamental properties of mono nanosheets have not been reported. Therefore, we have tried to measure such fundamental properties of mono nanosheets but still have a long way to obtain reliable data. Although the detailed band structure for the nanosheet p−n junction is still unclear, electron flow between CNO and NiO nanosheets during UV-light irradiation was confirmed by the photocurrent measurement.

■ CONCLUSIONS

Photocatalysts with ultrathin p−n junction structure were prepared with p-type and n-type two-dimensional semiconducting nanocrystals. LEIS spectra indicate that an ultrathin p−n junction (ca. 2 nm) was successfully prepared by the deposition of p-type and n-type 2D crystals. The photocatalytic activity on the n−p junction surface was higher than those on the p−n junction or p and n surfaces, verifying the strong influence of the junction structure. Kelvin probe force microscopy images showed that a potential gradient was generated on the surface of the p−n junction type photocatalyst, which is strongly influenced by not only the surface structure but also the layer under the surface. This indicates that material design to control the surface potential and potential gradient on the catalyst surface is necessary to obtain highly efficient photocatalysts. It is expected that the evaluation method and results presented here will contribute to the development of photocatalysts and improve understanding of the reaction mechanisms involved.

dx.doi.org/10.1021/ja409465k | J. Am. Chem. Soc. 2014, 136, 1872−1878

■ ASSOCIATED CONTENT

Supporting Information

Time courses of H_2 production from p-NiO, n-CNO, NiO/CNO (p−n), and CNO/NiO (n−p) junction films (S1) and Auger spectra mapping images of NiO/CNO junction film after photodeposition reaction (S2). This material is available free of charge via the Internet at http://pubs.acs.org.

■ AUTHOR INFORMATION

Corresponding Author

s-ida@cstf.kyushu-u.ac.jp

Notes

The authors declare no competing financial interest.

■ ACKNOWLEDGMENTS

We thank Dr. J. Druce and Prof. J. A. Kilner for discussion about LEIS data. This work was supported by JST PRESTO program and JSPS KAKENHI 70404324.

■ REFERENCES

(1) Gust, D.; Moore, T. A.; Moore, A. L. *Acc. Chem. Res.* **2009**, *42*, 1890.
(2) Kudo, A.; Miseki, Y. *Chem. Soc. Rev.* **2009**, *38*, 253.
(3) Wasielewski, M. R. *Acc. Chem. Res.* **2009**, *42*, 1910.
(4) Youngblood, W. J.; Anna Lee, S. H.; Maeda, K.; Mallouk, T. E. *Acc. Chem. Res.* **2009**, *42*, 1966.
(5) Asahi, R.; Morikawa, T.; Ohwaki, T.; Aoki, K.; Taga, Y. *Science* **2001**, *293*, 269.
(6) Zou, Z.; Ye, J.; Sayama, K.; Arakawa, H. *Nature* **2001**, *414*, 625.
(7) Kato, H.; Asakura, K.; Kudo, A. *J. Am. Chem. Soc.* **2003**, *125*, 3082.
(8) Maeda, K.; Teramura, K.; Lu, D.; Takata, T.; Saito, N.; Inoue, Y.; Domen, K. *Nature* **2006**, *440*, 295.
(9) Kanan, M. W.; Nocera, D. G. *Science* **2008**, *321*, 1072.
(10) Varghese, O. K.; Paulose, M.; LaTempa, T. J.; Grimes, C. A. *Nano Lett.* **2009**, *9*, 731.
(11) Wang, X.; Maeda, K.; Thomas, A.; Takanabe, K.; Xin, G.; Carlsson, J. M.; Domen, K.; Antonietti, M. *Nat. Mater.* **2009**, *8*, 76.
(12) Chen, X.; Liu, L.; Yu, P. Y.; Mao, S. S. *Science* **2011**, *331*, 746.
(13) Sakthivel, S.; Geissen, S. U.; Bahnemann, D. W.; Murugesan, V.; Vogelpohl, A. *J. Photochem. Photobiol., A* **2002**, *148*, 283.
(14) Chen, Y.; Crittenden, J. C.; Hackney, S.; Sutter, L.; Hand, D. W. *Environ. Sci. Technol.* **2005**, *39*, 1201.
(15) Long, M.; Cai, W.; Cai, J.; Zhou, B.; Chai, X.; Wu, Y. *J. Phys. Chem. B* **2006**, *110*, 20211.
(16) Kim, H. G.; Borse, P. H.; Jang, J. S.; Jeong, E. D.; Jung, O. S.; Suh, Y. J.; Lee, J. S. *Chem. Commun.* **2009**, 5889.
(17) Chen, C.; Cai, W.; Long, M.; Zhou, B.; Wu, Y.; Wu, D.; Feng, Y. *ACS Nano* **2010**, *4*, 6425.
(18) Yang, L.; Luo, S.; Li, Y.; Xiao, Y.; Kang, Q.; Cai, Q. *Environ. Sci. Technol.* **2010**, *44*, 7641.
(19) Yu, J.; Wang, W.; Cheng, B. *Chem. Asian J.* **2010**, *5*, 2499.
(20) Zhang, Z.; Shao, C.; Li, X.; Wang, C.; Zhang, M.; Liu, Y. *ACS Appl. Mater. Interfaces* **2010**, *2*, 2915.
(21) Zhang, S.; Sakai, R.; Abe, T.; Iyoda, T.; Norimatsu, T.; Nagai, K. *ACS Appl. Mater. Interfaces* **2011**, *3*, 1902.
(22) Meng, F.; Li, J.; Cushing, S. K.; Zhi, M.; Wu, N. *J. Am. Chem. Soc.* **2013**, *135*, 10286.
(23) Brongersma, H. H.; Draxler, M.; de Ridder, M.; Bauer, P. *Surf. Sci. Rep.* **2007**, *62*, 63.
(24) Kilner, J. A.; Skinner, S. J.; Brongersma, H. H. *J. Solid State Electrochem.* **2011**, *15*, 861.
(25) Schaak, R. E.; Mallouk, T. E. *Chem. Mater.* **2000**, *12*, 2513.
(26) (a) Ida, S.; Shiga, D.; Koinuma, M.; Matsumoto, Y. *J. Am. Chem. Soc.* **2008**, *130*, 14038. (b) Ida, S.; Takashiba, A.; Ishihara, T. *J. Phys. Chem. C* **2013**, *117*, 23357.
(27) Kikukawa, A.; Hosaka, S.; Imura, R. *Appl. Phys. Lett.* **1995**, *66*, 3510.
(28) Nowak, R.; Moraru, D.; Mizuno, T.; Jablonski, R.; Tabe, M. *Appl. Phys. Lett.* **2013**, *102*, No. 083109.